Solar internal rotation rate and the latitudinal variation of the tachocline

H. M. Antia[1], Sarbani Basu[2] and S. M. Chitre[1]

[1] *Tata Institute of Fundamental Research, Homi Bhabha Road, Mumbai 400 005, India*
[2] *Teoretisk Astrofysik Center, Danmarks Grundforskningsfond, Institut for Fysik og Astronomi,*
Aarhus Universitet, DK-8000 Aarhus C, Denmark

arXiv:astro-ph/9709083v1 10 Sep 1997

ABSTRACT
A new set of accurately measured frequencies of solar oscillations are used to infer the rotation rate inside the Sun, as a function of radial distance as well as latitude. We have adopted a regularized least squares technique with iterative refinement for both 1.5D inversion using the splitting coefficients and 2D inversion using individual m splittings. The inferred rotation rate agrees well with earlier estimates showing a shear layer just below the surface and another one around the base of the convection zone. The tachocline or the transition layer where the rotation rate changes from differential rotation in the convection zone to almost latitudinally independent rotation rate in the radiative interior is studied in detail. No compelling evidence for any latitudinal variation in position and width of tachocline is found though it appears that the tachocline probably shifts to slightly larger radial distance at higher latitudes and possibly becomes thicker also. However, these variations are within the estimated errors and more accurate data would be needed to make a definitive statement about latitudinal variations.

Key words: Sun: oscillations — Sun: interior — Sun: rotation

1 INTRODUCTION

The measured splittings of solar oscillation frequencies offer us a valuable tool for studying the rotation rate inside the Sun. It is possible to obtain both radial and latitudinal variation in the rotation rate (Schou, Christensen-Dalsgaard & Thompson 1994). Various techniques have been employed for inverting the splitting coefficients or even individual splittings in a multiplet (Brown et al. 1989; Gough & Thompson 1991; Pijpers & Thompson 1992; Sekii 1993; Wilson & Burtonclay 1995; Corbard et al. 1997).

The results obtained so far suggest that the observed surface differential rotation of the Sun persists through the convection zone (CZ). The rotation rate is nearly constant along different latitudes in most of the CZ, while in the radiative interior it is almost like rigid body rotation with a value intermediate between that of the solar equator and pole at the surface (cf., Thompson et al. 1996; Kosovichev et al. 1997). The transition occurs over a fairly thin layer, which is referred to as the "tachocline" (Spiegel & Zahn 1992). The thickness of the transition layer seems to be smaller than the best resolution that is currently achieved by inversion methods. This layer contains a substantial radial gradient of rotation velocity, of opposite signs in low and high latitudes. It is widely believed that the tachocline with its angular velocity gradients could be the seat of the dynamo responsi-

ble for the solar magnetic cycle (Weiss 1994; Gilman & Fox 1997). The introduction of a toroidal magnetic field in this layer with latitudinal differential rotation is naturally expected to lead to interesting consequences for the operation of the dynamo and its resultant manifestation in the solar surface activity. The strong gradient in the rotation rate is also expected to produce turbulence which is likely to mix material just below the convection zone — a phenomenon needed to match the structure of solar models with the helioseismically determined structure of the Sun (Richard et al. 1996; Basu 1997). The accurate measurement of solar internal rotation rate also provides strong constraints on the theory of angular momentum transport in the stellar interior (Rüdiger & Kitchatinov 1996), which should contribute to our understanding of the solar spin down over its lifetime.

In this work we investigate the internal rotation rate of the Sun, with particular emphasis on the tachocline. We have adopted the 1.5D inversion technique for inverting the rotation rate from the measured splitting coefficients (Ritzwoller & Lavely 1991; Schou, Christensen-Dalsgaard & Thompson 1994; Antia & Chitre 1996). We have also used a two-dimensional inversion of the individual frequency splittings themselves.

The location and structure of the tachocline is thus crucial in many models of the solar dynamo and it has been the subject of several detailed studies. Using a simple forward

modelling Kosovichev (1996) found that the tachocline is centered at a radial distance of $(0.692 \pm 0.005)R_\odot$ and with a width of $(0.09 \pm 0.04)R_\odot$, while Charbonneau et al. (1997) found it to be centered at $(0.704 \pm 0.003)R_\odot$ and with a width of $(0.050 \pm 0.012)R_\odot$. Similar results were also found by Basu (1997), who found that the tachocline is centered at $(0.7050 \pm 0.0027)R_\odot$ with a half-width of $(0.0098 \pm 0.0026)R_\odot$ which is $(0.0480 \pm 0.0127)R_\odot$ when scaled to the width as define by Kosovichev (1996) and Charbonneau et al. (1997) (see Section 3.1 for the definition of the width). Wilson, Burtonclay & Li (1996) find the tachocline to be somewhat deeper at $r = 0.68 \pm 0.01R_\odot$ and also slightly thicker $(0.12R_\odot)$. While all these results are roughly in agreement with one another, the differences in thickness are quite significant from the point of view of dynamo models as well as the hydrodynamical stability. Similarly, the exact location of tachocline with respect to the base of the convection zone is also crucial. Further, all these studies effectively assumed that the position and thickness of tachocline are independent of latitude. In this work, we attempt to find latitudinal variations in properties of the tachocline and also use improved data from GONG network to obtain better estimate for the tachocline properties. We use forward modelling techniques to detect possible latitudinal variation in properties of the tachocline. This includes the calibration method used by Basu (1997) and another technique based on simulated annealing.

For this work we have used a number of different data sets obtained by the Global Oscillations Network Group (GONG) project (Hill et al. 1996). These data are very precise and scan a large range of frequency and degree of modes. Apart from this we also use the data from BBSO (Woodard & Libbrecht 1993) combined with splitting coefficients for low degree modes as measured by BiSON (Elsworth et al. 1995).

The rest of the paper is organized as follows. In Section 2 we outline the methods used to invert the data to obtain the solar rotation rate and describe the inversion results. Techniques for determining whether there is any latitudinal variation in the tachocline are summarized in Section 3. In Section 4 we discuss results of inversion when the contribution from the tachocline is removed from the data before inversion and our conclusions are stated in Section 5.

2 INVERSIONS TO DETERMINE THE ROTATION RATE

The different modes of solar oscillations can be described by three integers: the radial order n, the angular degree ℓ and the azimuthal order m. The integers ℓ and m are the degree and order respectively of the spherical harmonic function used to describe the angular behaviour of the mode. In a spherically symmetric, non-rotating star, the frequency $\omega_{n,\ell,m}$ of an eigenmode is independent of m and the mode is $(2\ell+1)$-fold degenerate. The spherical symmetry of the Sun is broken by rotation, lifting the degeneracy of the modes. The differences in frequency of modes with the same n and ℓ, but different m, can be related to the rotation rate in the

Sun by

$$
\begin{aligned}
D_{n,\ell,m} &= \frac{\omega_{n,\ell,m} - \omega_{n,\ell,-m}}{2m} \\
&= \int_0^{R_\odot} \int_{-1}^1 dr \, d\cos\theta \, K_{n,\ell,m}(r,\theta)\Omega(r,\theta),
\end{aligned}
\tag{1}
$$

where the kernels $K_{n,\ell,m}(r,\theta)$ are defined by Pijpers (1997).

Most helioseismic data sets do not contain frequencies of individual modes or the individual splittings $D_{n,\ell,m}$ as defined by equation (1), but rather frequencies of modes for a given (n,ℓ) are expressed as sum of polynomials in m, namely,

$$
\omega_{n,\ell,m} = \omega_{n,\ell} + \sum_{s=1}^{s_{\max}} c_s^{(n,\ell)} \mathcal{P}_s^{(\ell)}(m),
\tag{2}
$$

where $\mathcal{P}_s^{(\ell)}(m)$ are suitable polynomials of degree s, and generally, $s_{\max} < 2\ell$. For a proper choice of the polynomials, the individual inversion problems for each splitting coefficient $c_s^{(n,\ell)}$ becomes decoupled from the rest (Ritzwoller & Lavely 1991).

The data from the GONG instrument are available as frequencies of all individual modes, as well as splitting coefficients for the polynomials as defined by Ritzwoller & Lavely (1991). We adopt both these forms of data, and use the so-called 1.5D inversion method (described below) to invert the data in the form of splitting coefficients. This method has the advantage of being efficient in terms of computing resources. However, in order to exploit the full potential of the data we need to invert the individual frequency splittings directly using a two dimensional inversion method.

2.1 The 1.5D inversion

The rotational splitting coefficients are sensitive only to the component of rotation velocity that is symmetric about the equator and we therefore assume the rotation velocity to be symmetric. In order to determine the latitudinal dependence of the rotation rate, we follow Ritzwoller and Lavely (1991) and express the rotation velocity as

$$
v_{\rm rot}(r,\theta) = \Omega(r,\theta) r \sin\theta = -\sum_{s=0}^\infty w_{2s+1}(r) \frac{\partial}{\partial\theta} Y_{2s+1}^0(\theta), \tag{3}
$$

where θ is the colatitude, $Y_k^0(\theta)$ are the spherical harmonics and $w_s(r)$ are expansion coefficients which are related to the splitting coefficients $c_s^{(n,\ell)}$ (cf., equation (2)) by

$$
c_s^{(n,\ell)} = \int_0^{R_\odot} w_s(r) K_s^{(n,\ell)}(r) r^2 \, dr,
\tag{4}
$$

where the kernels $K_s^{(n,\ell)}(r)$ are given by (Ritzwoller & Lavely 1991)

$$
K_s^{(n,\ell)} = -\frac{\rho_0}{r} \frac{(\xi_r^2 + \ell(\ell+1)\xi_h^2 - 2\xi_r\xi_h - \frac{1}{2}s(s+1)\xi_h^2)}{\int_0^{R_\odot} \rho_0(\xi_r^2 + \ell(\ell+1)\xi_h^2) r^2 \, dr}.
\tag{5}
$$

Here, $\rho_0(r)$ is the density in the equilibrium solar model, while ξ_r and ξ_h are respectively, the radial and horizontal components of displacement eigenfunctions. Using the splitting coefficients $c_s^{(n,\ell)}$ from the GONG data, equation (4) can be inverted to obtain $w_s(r)$. The advantage of this choice

for expansion is that the resulting inverse problems for determining the individual components $w_1(r)$, $w_3(r), \ldots$ get decoupled and each component can be estimated independently. The components $w_s(r)$ are calculated by solving separate one-dimensional inversion problems with the iterative refinement of the regularized least squares solution (Antia, Chitre & Thompson 1996). The rotation rate at any given radial distance and colatitude can then be computed using equation (3).

We use cubic B-spline basis functions to represent the rotation rate and the regularized least squares inversion is performed using the singular value decomposition. The B-splines are defined over a set of 50 knots which are uniformly spaced in acoustic depth. We have used only the first 6 terms of the expansion (3), as the higher splitting coefficients in the GONG data appear to be dominated by random noise. The observed rotational splitting coefficients from GONG data for $\ell \leq 150$ and $1 \leq \nu \leq 3.5$ mHz are used for inversion. Further, in actual practice we directly find the individual components of rotation rate as defined by

$$\Omega_s(r) = \sqrt{\frac{2s+1}{4\pi}} \frac{w_s(r)}{r}, \tag{6}$$

instead of $w_s(r)$.

Since the inversion problem defined by equation (4) is in general ill-conditioned, some regularization or smoothing is required to obtain any meaningful solution in the presence of errors in observed data sets. In order to study the sensitivity of inversion results on smoothing prescription, we have tried three different prescriptions for the regularized least squares inversion: (i) First derivative smoothing, where we minimize

$$\sum_{n,\ell} (\sigma_s^{(n,\ell)})^{-2} \left[c_s^{(n,\ell)} - \int_0^{R_\odot} K_s^{(n,\ell)}(r) w_s(r) r^2 \, dr \right]^2$$
$$+ \lambda \int_0^{R_\odot} \frac{1}{r} \left(\frac{dw_s}{dr} \right)^2 \, dr, \tag{7}$$

Here $c_s^{(n,\ell)}$ are the observed splitting coefficients and $\sigma_s^{(n,\ell)}$ the corresponding error and λ is the regularization parameter. For this case, the rotation rate in the solar core — where the amount of information is rather meager as the splitting data for low degree modes have large errors — tends to a constant value when sufficient smoothing is applied.

(ii) Second derivative smoothing, where we use the second derivative instead of the first in the second term of equation (7). In this case, the rotation rate in the solar core tends to a monotonic linear profile, which is perhaps unrealistic as it may keep rising or falling depending on the gradient. In order to overcome this problem we apply the following boundary conditions at the center:

$$\frac{d\Omega_i}{dr} = 0,$$
$$\Omega_i(0) = 0 \quad (i > 1). \tag{8}$$

The second boundary condition may have some justification, as there is no information available to determine the higher order coefficients $\Omega_i(r)$ $(i > 1)$ in the solar core from the splitting data. This is because only the first splitting coefficient c_1 is known from observations for the low degree modes which sample the solar core . This condition is also required
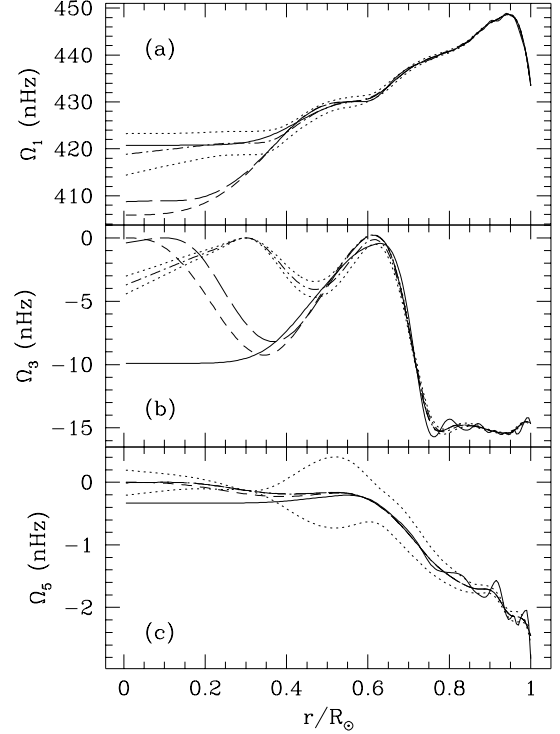
Figure 1. The first three components of the rotation rate obtained with different prescriptions of smoothing. In all three panels the continuous line is the result obtained with first derivative smoothing. The short-dashed, long-dashed and dot dashed line are for second-derivative smoothing with the boundary conditions (equation (8)) applied at $r = 0$, 0.1 and $0.3R_\odot$ respectively. The dotted lines show 1σ errors on solution obtained with the second derivative smoothing and boundary conditions applied at $0.3R_\odot$.

to ensure regularity of rotation velocity at the origin (Corbard et al. 1997).

(iii) This is same as (ii) except that the boundary conditions given by equation (8) are applied at a radial distance $r = 0.3R_\odot$ (or $r = 0.1R_\odot$). These boundary conditions essentially try to constrain the rotation rate to become constant in the region inside where the boundary conditions are applied. This may be justified as we do not appear to have enough information to determine the gradient in rotation rate in the core (cf., Chaplin et al. 1996).

In all these cases, the method of iterative refinement effectively chooses the regularization parameter λ as explained by Antia, Chitre & Thompson (1996). It is found that the regularization parameter increases with the order s of the splitting coefficient, which probably reflects the fact that higher order coefficients are dominated by noise in most regions.

2.1.1 Results of 1.5D inversion

We use the 1.5D inversion technique outlined above to infer the rotation rate in the solar interior using the GONG data for months 4–14, which consists of splitting coefficients for modes with $\ell \leq 150$. The χ^2 per degree of freedom is found to be close to unity (between 1.1–1.2) in all cases. In order to study the influence of smoothing on the inversion results we perform inversion using different smoothing prescriptions given in Section 2.1 and the results are displayed

in Fig. 1. This shows the rotation rate corresponding to the first three splitting coefficients c_1, c_3 and c_5. From the figure it is clear that the results in the convection zone are not very sensitive to the choice of smoothing or to the point at which the boundary conditions given in equation (8) are applied. Noticeable differences are seen only for those parts of the Sun where the data have large errors. The maximum difference of about 10 nHz occurs in the core in the latitudinally independent component Ω_1. Similar differences are seen for the component Ω_3 also. These differences are comparable to the error estimate in the inversion results arising from errors in observed splitting coefficients. It may be noted that the error estimates shown in the figure for the second derivative smoothing with the boundary conditions applied at $r = 0.3R_\odot$ show a decrease in the core. This is artificial, and is entirely the result of boundary conditions. In reality the errors should increase rapidly as r decreases in the core. Some of the differences in the core between the results using first and second derivative smoothing are due to absence of boundary conditions in the first derivative case. However, a part of the difference may also be due to possible systematic errors in splitting coefficients of the low degree modes. From this figure it is clear that for $r > 0.5R_\odot$ the choice of smoothing or the point where the boundary conditions are applied does not make significant difference and in most of the work we have confined ourselves to this region. All the following results using 1.5D inversion have been obtained using second derivative smoothing with the boundary conditions applied at $0.3R_\odot$.

In order to study the sensitivity of the inversion technique to possible systematic errors in the input data sets we have repeated the inversion for various sets of GONG data and the results are shown in Fig. 2. This figure also includes the results obtained using the averaged BBSO data for years 1986, 1988, 1989 and 1990 (Woodard & Libbrecht 1993), combined with the splittings for low degree modes from BiSON (Elsworth et al. 1995). It is clear that there is some systematic difference between different data sets, but the difference is comparable to the error estimates arising from inversions. This difference is also comparable to that arising from different smoothing prescriptions as displayed in Fig. 1. The spread between various curves in Fig. 2 should give an estimate of expected errors in inverted profiles, including those arising from systematic errors in the input data. It may be noted that the data from GONG month 10, GONG months 4–7 and BBSO+BiSON have larger errors as compared to that in the GONG months 4–14 data and this is reflected in tachocline region where the GONG months 4–14 data appear to have higher resolution and hence the tachocline is sharper.

A contour diagram showing the rotation rate inside the Sun as inferred using the GONG months 4–14 data is shown in Fig. 3. It can be seen that the rotation rate is approximately constant along radial lines in the convection zone. These results are similar to earlier inversions for rotation rate (Thompson et al. 1996; Kosovichev et al. 1997). The tachocline is clearly visible in these contour diagram. Apart from the tachocline there, is another shear layer near the solar surface where the rotation rate increases with depth. This shear layer appears to extend to all latitudes and the rotation rate increases by about 17 nHz in this layer at the equator, but the change is lower at higher latitudes. The
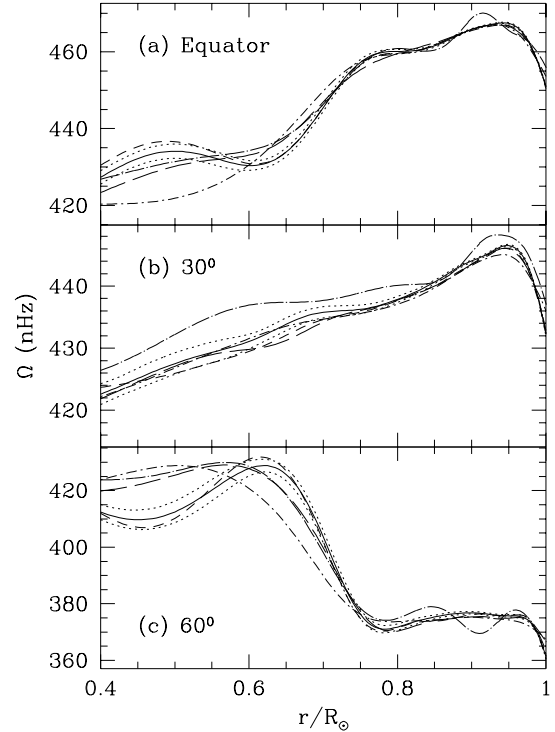

Figure 2. Solar rotation rate at the equator, 30° and 60° latitudes obtained using different data sets. In all three panels, the continuous lines are the results obtained using the GONG months 4–14 data with the dotted lines showing the 1σ error limits. The short-dashed, long-dashed and dot-short dashed lines are for GONG months 4–10, months 4–7 and month 10 data respectively, while the dot-long dashed line is for the BBSO+BiSON data combination. Note that while for all the GONG data sets we have used splitting coefficient from c_1 to c_{11}, for the BBSO+BiSON set we have used only the data up to c_5.

maximum value of rotation rate occurs around $r = 0.95R_\odot$. The maximum rotation rate at the equator is 467.5 ± 0.2 nHz at $r = 0.945R_\odot$. The inverted rotation rate at the solar surface is close to that inferred from Doppler measurements (Snodgrass 1992). The rotation rate in the radiative interior is more or less constant and some of the features seen in the contour diagram do not appear to be significant. Although there is considerable uncertainty in the estimate of the rotation rate in the core, but it appears to be less than the surface equatorial rotation rate.

2.2 2D inversion

Although the 1.5D inversion technique described in Section 2.1 is very efficient in terms of computing resources, it is not clear if the expansion of rotation rate given by equation (3), imposes any limitation on the solution. A possible drawback of 1.5D inversion is the loss of information, since the number of splitting coefficients is generally much smaller than the number of individual splittings, but it is not clear if the individual splittings contain any more information than the first few splitting coefficients. A more serious problem occurs in the inversion of higher order coefficients, which have useful information only in the outer part of the convection zone and as a result the solution in most of the interior is essentially determined by the applied smoothing
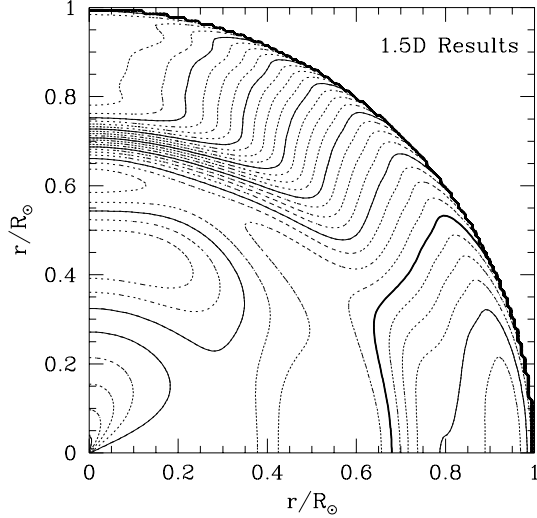
Figure 3. A contour diagram of the solar rotation rate as obtained by the 1.5D inversion technique using GONG months 4–14 data. Due to the symmetry of the inversion results, the rotation rate has been shown for just one quadrant only. The dotted contours have been drawn at intervals of 5 nHz., and the continuous ones at intervals of 20 nHz. The thick continuous line is the contour at a level of 440 nHz. The x-axis represents the solar equator while the y-axis represents the rotation axis.

and boundary conditions. A 2D representation of rotation rate will hopefully be able to overcome this problem. Another drawback of the 1.5D inversion is that all components $\Omega_s(r)$ make their maximum contribution at the pole and further this maximum value is much larger than that in other regions. This is particularly true for the higher order components. As a result, the errors in the 1.5D inversions tend to get highly magnified near the pole and may even give rise to spurious features if very high order terms are included. In order to overcome these problems we attempt a 2D inversion technique which does not use the expansion given by equation (3), but instead directly represents the two dimensional function $\Omega(r, \theta)$ in terms of suitable basis functions.

In order to solve the inversion problem defined by equation (1) we represent the rotation rate in terms of B-spline basis functions in r and θ,

$$\Omega(r, \theta) = \sum_{i=1}^{n_r} \sum_{j=1}^{n_\theta} b_{ij} \phi_i(r) \psi_j(\cos \theta), \qquad (9)$$

where b_{ij} are the coefficients of expansion and $\phi_i(r)$ are the B-spline basis functions over r and $\psi_j(\cos \theta)$ are those over $\cos \theta$, n_r and n_θ are the number of basis functions in r and $\cos \theta$ respectively. We use a set of knots which are uniformly spaced in acoustic depth and $\cos \theta$ respectively to define $\phi_i(r)$ and $\psi_j(\cos \theta)$.

This inversion problem is also solved using the regularized least squares technique with iterative refinement. In this case, we have used only second derivative smoothing,
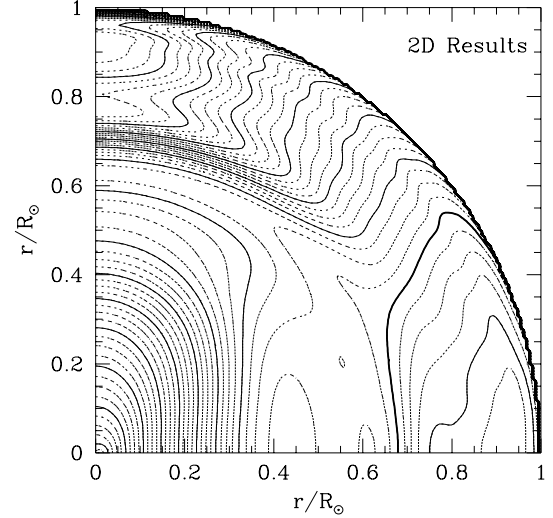
Figure 4. A contour diagram of the solar rotation rate as obtained by the 2D inversion of individual splittings using GONG months 4–14 data. The format is the same as that for Fig. 3.

which involves minimizing

$$\sum_{n,\ell,m} \sigma_{n,\ell,m}^{-2} \left[D_{n,\ell,m} - \int_0^{R_\odot} dr \int_{-1}^1 d \cos \theta K_{n,\ell,m}(r, \theta) \Omega(r, \theta) \right]^2$$

$$+ \lambda_r \int_0^{R_\odot} dr \int_{-1}^1 d \cos \theta r^{-1} \left(\frac{\partial^2 \Omega}{\partial r^2} \right)^2$$

$$+ \lambda_\theta \int_0^{R_\odot} dr \int_{-1}^1 d \cos \theta \sin^2 \theta \left(\frac{\partial^2 \Omega}{\partial \cos \theta^2} \right)^2, \qquad (10)$$

where, λ_r and λ_θ are the two regularization parameters controlling the smoothing. No boundary conditions are applied in this case to constrain the rotation rate in the core. We have used 50 knots in r and 30 knots in $\cos \theta$ to represent the rotation rate.

It is also possible to perform 2D inversion for splitting coefficients, (Schou, Christensen-Dalsgaard & Thompson 1994; Pijpers 1997) where the rotation rate is expressed in terms of 2D basis functions (equation (9)) and appropriate combinations of individual splittings are constructed to relate the corresponding splitting coefficients to the rotation rate. In order to see whether the differences between the 1.5D and 2D results are due to the expansion of rotation rate or the data, we have done a two-dimensional inversion for the splitting coefficients also. Thus we have two sets of results using 2D inversions, one for 2D inversion of individual splittings $D_{n,\ell,m}$, and the other for 2D inversion of the splitting coefficients $c_s^{(n,\ell)}$.

2.2.1 Results of 2D inversion

A contour diagram of the rotation rate inferred by 2D inversion of GONG months 4–14 data, comprising of about 85000 splittings of individual modes is shown in Fig. 4. The χ^2 per degree of freedom in this case is around 1.3. Note that inside the CZ, the results are essentially similar to that obtained by the 1.5D method, despite having a much larger number of splittings in 2D inversion. Thus it appears that the data are well represented by the 6 splitting coefficients. However, in the radiative interior the solutions obtained using 1.5D and
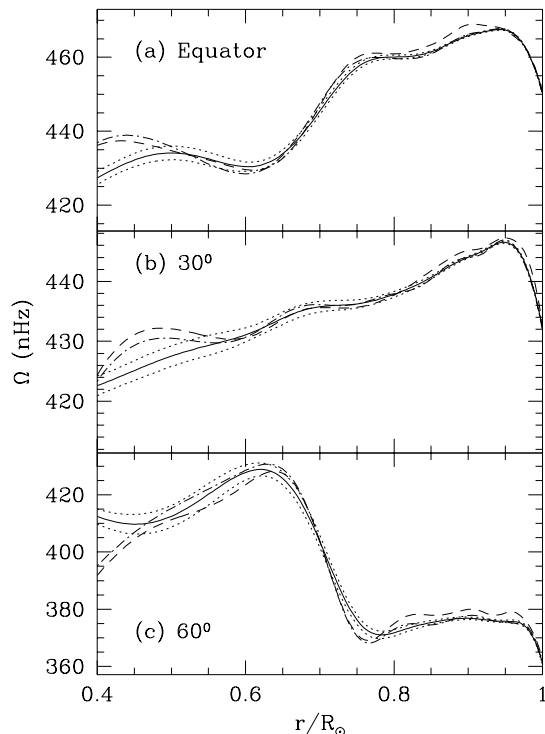
6

Figure 5. Comparison of the rotation inversion results at fixed latitude obtained by the 1.5D and 2D inversion methods. The continuous line shows the results obtained by the 1.5D inversion method with the dotted lines showing the 1σ error limits. The dashed line are those obtained by the 2D inversion of the individual splittings and the dot-dashed line are those obtained by the 2D inversion of the splitting coefficients.

Figure 6. Comparison of the rotation inversion results at fixed radius. The line styles are the same as in Fig. 5. In the top panel the heavy short dashed- long dashed line shows the observed surface rotation rate as estimated by Doppler measurements (Snodgrass 1992).

2D inversions are significantly different. A large part of the difference is due to the boundary conditions imposed in the 1.5D inversion which along with the smoothing, tend to produce solid body rotation in the interior. In the absence of any boundary condition, the 2D inversion technique attempts to fit the splittings for low degree modes which probably have some systematic errors, and produces a sharply decreasing rotation rate in the radiative interior. This decrease may not be real as it could result from second derivative smoothing coupled with errors in data.

It appears that the behaviour of the solutions in the polar regions is also somewhat different. The 2D-solution shows a rapid decrease of the rotation rate towards the pole similar to that seen in the data from the MDI instrument on board the SOHO spacecraft. The 1.5D result also shows a decrease in the surface rotation rate at the pole, but the reduction is not as much as in 2D inversion of individual splittings. The errors in inversion increase rapidly with latitude near the pole and as a result it is difficult to discern any features at high latitudes reliably. Thus the differences at high latitudes possibly reflect our inability to obtain reliable inversion results in that region. However, from the form of expansion of rotation rate (equation (3)) in 1.5D inversion, it is clear that contribution of each component (Ω_i) has a strong maximum at the pole and any error in these components will be highly magnified there. This is particularly true of the higher order terms in the expansion. It thus appears that 2D inversion of individual splittings, which does not assume any particular expansion of rotation rate, may be able to give better re-
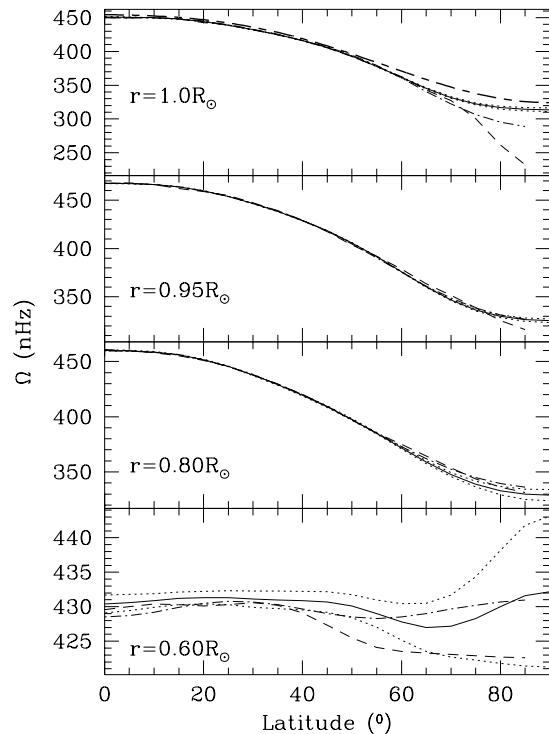
sults near the pole, though the errors will still be large and the smoothing will play a dominant role in determining the solution near the poles.

In order to see whether the differences between the 1.5D and 2D results are due to the representation of rotation rate or the data, we have also done a two dimensional inversion of the splitting coefficients. For this we use the same splitting coefficients as were used in the 1.5D inversion but expand the rotation rate in terms of 2 dimensional basis functions using equation (9). These results are also shown in Figs. 5 and 6. Note that in the outer layers of the Sun the results of the 1.5D and two-dimensional inversion of splitting coefficients are very close to each other, but slightly different from the results of the 2D inversion of the individual splittings. In the deeper layers however, the results of 1.5D inversion are quite different from both the 2D inversions. As already discussed this is due to the boundary conditions (equation (8)) that are applied in the 1.5D inversion method.

3 THE TACHOCLINE

It can be seen from the results of the inversions that there is a sharp transition close to the base of the convection zone where the rotation rate changes from differential rotation in the convection zone to a rotation rate that is almost independent of latitude. Since the inversions are not able to resolve the tachocline, other techniques have been employed to study this shear layer. Even though inversions indicate that the tachocline is slightly shallower and thicker at high latitudes, it is not clear if this represents a real variation or
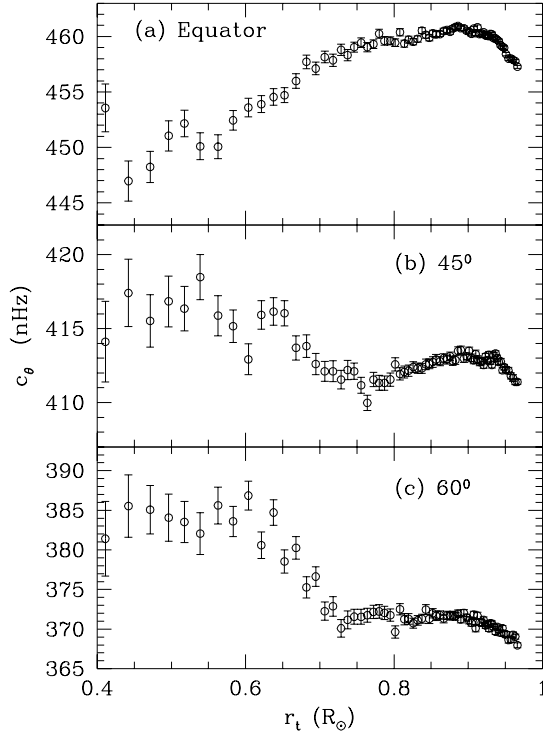
Figure 7. The splitting coefficients for GONG months 4–14 combined to obtain the data for different latitudes, which are marked in the figure. The points represent the combinations binned in groups of 15.

is just an artifact of inversion technique caused by the fact that the extent of jump increases with latitude and the resolution of inversion techniques deteriorates with increasing latitude. For an independent confirmation of this variation we construct combinations of rotational splitting coefficients $c_s^{(n,\ell)}$, which give the rotation velocity at some predefined co-latitude θ_0. Thus multiplying equation (4) by $dY_s^0/d\theta|_{\theta=\theta_0}$ and summing over s we get

$$\sum_{s=0}^{\infty} c_{2s+1}^{(n,\ell)} \left.\frac{dY_{2s+1}^0}{d\theta}\right|_{\theta=\theta_0} = -\int_0^{R_\odot} v_{\rm rot}(r,\theta_0) K^{(n,\ell)}(r) r^2 \, dr. \quad (11)$$

Here, in principle, the kernel $K^{(\ell,n)}(r)$ also depends on s, but for simplicity we neglect the s dependence, since the s-dependent term is in general very small, as can be seen from equation (5). With this approximation equation (11) reduces to an one dimensional inversion problem at fixed latitude. Since inversion cannot resolve the tachocline, we use a forward modeling technique to estimate the parameters defining the tachocline.

We have first made the appropriate combinations of the splittings data for different latitudes using the coefficients c_1–c_{11}. Fig. 7 shows the data, binned in groups of 15 modes, plotted as a function of the lower turning point. We show the data at the equator, $45°$ and $60°$ latitudes. Note that the equator shows some hint of a jump, while $45°$ and $60°$ latitudes show a clear jump. We concentrate on the latitudes which show evidence of the transition and try to determine the magnitude of the jump, position and thickness of the transition at latitudes of $0°, 15°, 45°, 60°$ and $75°$. The data for the $30°$ latitude does not give any clear indication of the transition, which is consistent with inversion results. The

latitudinal variation of the magnitude of the jump is obvious from the figure, but the change in position and thickness are not clear. We use both the calibration method used by Basu (1997) and another method based on simulated annealing to study the tachocline at each latitude separately.

Apart from this we have also tried a 2D fit with some assumed form for tachocline with latitudinal variation to simultaneously fit all the splitting coefficients for obtaining the latitudinal variation in the properties of the tachocline.

3.1 Calibrating the tachocline

The method followed here is the same as that used by Basu (1997). Data on frequency splittings for modes trapped in the convection zone and those with turning points around the CZ base are quite precise. The exact position and thickness of the tachocline can be determined by calibrating the difference in splittings between the Sun and models with known position and thickness of the tachocline. While Basu (1997) assumed that the position and thickness of the tachocline can be determined by the splitting coefficient c_3 alone, which automatically ensures that the position and thickness of tachocline are independent of latitude. In this work, we explicitly study the latitudinal variation by applying the same procedure to data for each of the chosen latitudes.

In order to estimate the position, thickness and the jump in the tachocline we construct a series of models with known properties. We parameterize the calibration models with the rotation profile:

$$\Omega_{\rm cal} = \frac{\delta\Omega}{1 + \exp[(r_d - r)/w]}, \quad (12)$$

where $\delta\Omega$ is the jump in the tachocline, w is the half-width of the transition layer, and r_d the mid-point of the transition region. Thus the rotation rate increases from a factor $1/(1+e)$ of its maximum value to the factor $1 - 1/(1 + e)$ of its maximum value in the range $r = r_d - w$ to $r = r_d + w$. The models described by equation (12) have almost zero rotation rate in the core, which is, of course, not true for the Sun. To take this into account we subtract the contribution of a uniform rotation rate Ω_c, the estimated value of rotation rate in the interior as obtained from the inversion results, from the observed splittings.

Note that our parameterisation of the tachocline is different from that of Kosovichev (1996) and Charbonneau et al. (1997). The definition of the position and the jump remains the same, the thickness of the tachocline as defined by them is roughly 4.9 times the half-width we have defined, i.e. a half-width of $0.01R_\odot$ in our model corresponds to a thickness of $0.049R_\odot$ in their models. Thus the tachocline thickness of $(0.050 \pm 0.012)R_\odot$ as estimated by Charbonneau et al. (1997) using their model will be equivalent to a half-width of $(0.0102\pm0.0025))R_\odot$ by our definition, which is consistent with the value of $(0.0098\pm0.0026)R_\odot$ determined by Basu (1997). Of course, the form of variation in rotation rate inside the tachocline can only be verified by inversions, which do not at present have the required resolution. However, as long as the thickness of tachocline is small enough, the exact form of variation within this layer may not be important, as is seen by the similarity of the results obtained by Charbonneau et al. (1997) and Basu (1997).

If c_θ be the combination of observed splitting coefficients for a given latitude (after removing the contribution from Ω_c) and a_θ that of the calibration model, then to determine the jump, we make the following fit by treating the splittings as a function of the lower turning point, r_t, of the mode:

$$c_\theta(r_t) = \alpha a_\theta(r_t) + \phi(r_t), \qquad (13)$$

where α is the factor determining the jump and $\phi(r_t)$ is a low degree polynomial which takes into account any trend in the real rotation rate not taken into account by the parameterisation in equation (12). The constant term in this polynomial will also take care of differences arising due to use of incorrect Ω_c while subtracting out the contribution from core rotation rate. A polynomial of degree 2 is found to be sufficient. The fit is made between r_t of 0.6 and 0.9 $R_\odot$. Modes with lower turning point are avoided because of large observational errors in these modes. Modes with higher r_t are not used so that shear layer known to exist just below the solar surface does not affect the results. We perform a least squares fit with the weights for each mode being the inverse of the errors in the corresponding splitting.

We follow exactly the same procedure as that of Basu (1997) for determining the position and thickness of the tachocline. To recapitulate briefly, the difference in the splitting coefficients between a model and similar models which have discontinuities at different positions have a well defined peak and the height of the peak is proportional to the difference in the positions of the discontinuity. Thus the peak height can be calibrated to find the position of the discontinuity. If the models are not similar, e.g., have different trends in the convection zone or in the interior, or have a different width of transition, the peak lies on a smooth part which can be represented as a low degree polynomial. A similar calibration can be used to estimate the thickness over which the transition of the rotation rate occurs. In this case the width of the peak between two models is proportional to the thickness of the wider transition, but a simple scaling of the radius around the peak position can reduce the curves to similar widths.

We have constructed models with r_d of 0.68, 0.69, 0.70, 0.71 and 0.72 $R_\odot$ and half-width w of 0, 0.005, 0.01, 0.015, 0.02 and 0.025 $R_\odot$. We have used $\delta\Omega$ of 20 nHz in the calibration models and determined the actual jump from the splittings as outlined earlier. The splittings in the calibration models are then scaled to the required jump.

For the purpose of calibration, we consider the difference in the splitting coefficients between neighbouring calibration models and fit a spline through the points

$$\Phi(r) = \delta a(r) = \sum_i a_i \psi_i(r), \qquad (14)$$

where the $\Phi(r)$'s are the calibration curves and $\psi(r)$ are the cubic B-spline basis-functions. Thus we have 4 calibration curves from the 5 calibration models.

The difference in splittings between each calibration model and the observed splittings can be fitted with the form

$$\delta c_\theta = c_\theta(r) - a_\theta(r) = \alpha \Phi(r) + f(r). \qquad (15)$$

Here $\Phi(r)$ is the calibration curve defined in equation (14) and $f(r)$ is a low degree polynomial used to take into account

systematic effects arising from differences in other parameters, like width etc. between the observations. As in Basu (1997) we find that a polynomial of degree two or three is optimum. The constant α and the coefficients of the polynomial $f(r)$ are obtained by a least-squares fit to the data. In practice, we determine α for all five calibration models and interpolate to find the points where $\alpha = 0$. The four calibration curves give four results which are then averaged.

Ideally, $\delta\Omega$, r_d, and w should be determined simultaneously, however, for simplicity in this work we determine these parameters by independent fits. It has been shown by Basu (1997) that statistical errors arising from uncertainties in observed splittings dominate over the systematic errors, and therefore, such a procedure may not introduce significant additional errors. To try and keep the parameters of the calibration models close to that of the actual tachocline, the fit in practice is done in two steps. We first determined the positions and widths of the tachocline at the different latitudes using the models with parameters found for the coefficient c_3 by Basu (1997). The process was repeated with calibration models constructed with parameters closer to those determined in the first round of fits.

Note that the models defined by equation (12) have a flat rotation rate in the CZ, which is obviously not the case at all latitudes. This is taken care of in our fitting process described above through the smooth part, $\phi(r)$ in equation (13) and $f(r)$ in equation (15). However, in order to check how much difference the flat rotation rate in the CZ makes, we have also constructed calibration models where the rotation rate in the CZ follows the trend revealed by the inversions described in the previous section. In addition to the form shown in equation (12), these models have latitude dependent extra terms, with rotation rate defined as:

$$\Omega = \begin{cases} \Omega_{\text{cal}} + B(r - 0.7) & \text{if } r \leq 0.95 \\ \Omega_{\text{cal}} - C(r - 0.95) + 0.25B & \text{if } r > 0.95 \end{cases} \qquad (16)$$

Here, the coefficients B and C are obtained from the inversion results and the term Ω_{cal} is defined by equation (12). The models described by equation (16) use an approximate value of the jump; we still use the fit in equation (13) to find the exact magnitude of the jump. The procedure to find the position and thickness of the tachocline remains the same. It must be noted that for these models, the polynomial ϕ of equation (13) and $f(r)$ in equation (15) are very small.

For all cases, the error estimates in the tachocline parameters are obtained using Monte-Carlo simulations. We have used two sets of GONG data, those from GONG months 4–10 and GONG months 4–14 for the present work.

3.2 The method of simulated annealing

The calibration method described above suffers form the disadvantage that each parameter defining the tachocline is determined separately when the rest of the parameters are held fixed. We therefore tried another forward modeling method, where the jump, position and width can be found simultaneously. Since this will require a nonlinear least squares fit, we have resorted to the method of simulated annealing, which has better chance for finding the global minimum. For this purpose the rotation rate at any given latitude is parame-

terized by

$$\Omega_{\mathrm{ann}}(r) = \begin{cases} \Omega_c + B(r - 0.7) \\ \quad + \frac{\delta\Omega}{1 + \exp[(r_d - r)/w]} & \text{if } r \leq 0.95 \\ \Omega_c + 0.25B - C(r - 0.95) \\ \quad + \frac{\delta\Omega}{1 + \exp[(r_d - r)/w]} & \text{if } r > 0.95 \end{cases} \quad (17)$$

where Ω_c, B, C are the three parameters defining the smooth part of rotation rate while $\delta\Omega$, r_d and w define the tachocline. Here B is the average gradient in the lower part of convection zone, while C is the gradient in the near surface shear layer. These six parameters are determined by a non-linear least squares fit to the combinations of splitting coefficients representing the rotation rate at the required latitude. Once again we use only those modes which have turning points in the range 0.6–$0.9R_\odot$ in this fit. We use the method of simulated annealing (Vanderbilt & Louie 1984; Press et al. 1993) to minimize the χ^2 function. Since there are likely to be many local minima where the minimization tends to get trapped, even with simulated annealing, we make 20 attempts using different sequence of random numbers in the annealing procedure to find the minimum and accept the one that gives the lowest χ^2.

Instead of fitting the rotation rate at each latitude separately and then finding the variation in the tachocline properties, we can directly fit a 2D form of rotation rate with tachocline to obtain this variation. The form fitted is the same as in the 1D case (equation (17)) with the following substitutions

$$\begin{aligned} B &= B_1 + B_3 P_3(\theta) + B_5 P_5(\theta), \\ \delta\Omega &= \delta\Omega_1 + \delta\Omega_3 P_3(\theta) + \delta\Omega_5 P_5(\theta), \\ r_d &= r_{d1} + r_{d3} P_3(\theta), \\ w &= w_1 + w_3 P_3(\theta), \end{aligned} \quad (18)$$

where

$$\begin{aligned} P_3(\theta) &= 5\cos^2\theta - 1, \\ P_5(\theta) &= 21\cos^4\theta - 14\cos^2\theta + 1, \end{aligned} \quad (19)$$

are polynomials used to define the latitude dependence. We have used these polynomials so as to ensure some degree of separation between contributions to various splitting coefficients. This introduces 5 parameters to define the smooth part and another 7 parameters to define the tachocline. It is not clear if all these parameters are required to explain the data and we have carried out experiments involving different combinations to determine which of these parameters are required. Once again we use the simulated annealing technique to simultaneously fit the first 3 splitting coefficients c_1–c_5 for all modes with lower turning point in the range 0.6–$0.9R_\odot$. The reason for using only the first 3 splitting coefficients is that with the assumed form for tachocline model given by equation (18), we do not expect to fit the higher coefficients properly. If these coefficients are to be fitted then additional parameters will need to be introduced in $\delta\Omega$ and B in equation (18). We have tried this also but we do not think that the fits with additional parameters and coefficients are any better than the ones considered here as the higher order parameters turn out to be rather small. As a result, in this work we present the results obtained by fitting only the first three splitting coefficients.
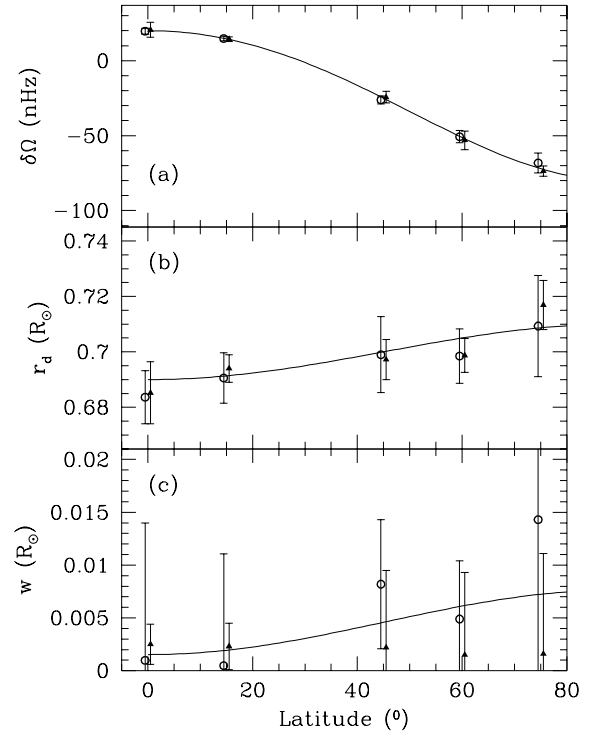

Figure 8. A summary of the tachocline results for the test model. Panels (a),(b) and (c) show the results of the jump, position and half-width respectively. In each panel the continuous line represents the exact value. The circles show the results of the calibration method and the triangles are the results obtained by 1D annealing. The symbols are displaced by $\pm0.5°$ about the true latitude for the sake of clarity. In panel (c) the actual width has been scaled down by a factor of 3.25 to account for the difference in form of variation within the tachocline.

3.3 Results

In order to test the procedure outlined above we constructed a test model with prescribed rotation rate including a tachocline and applied the techniques for determining the properties. The rotation rate in the test model was chosen to be

$$\begin{aligned} \Omega(r,\theta) = {}& 430 + 20\sin(\pi r/2) \\ & + 10(1 - 4\cos^2\theta - \cos^4\theta)F_j(r), \end{aligned}$$

$$F_j(r) = \begin{cases} -1 & \text{if } r < r_d - w \\ \sin(0.5\pi(r - r_d)/w) & \text{if } r_d - w \leq r \leq r_d + w \\ +1 & \text{if } r > r_d + w \end{cases} \quad (20)$$

$$\begin{aligned} r_d &= (0.69 + 0.02\cos^2\theta)R_\odot, \\ w &= (0.005 + 0.02\cos^2\theta)R_\odot. \end{aligned}$$

The splitting coefficients computed for this model were perturbed by adding random errors with the same distribution as that specified by quoted errors in the GONG months 4–14 data. The perturbed data were then used to infer the characteristics of the tachocline and the results using the calibration and 1D annealing methods are shown in Fig. 8. Since this model has a different form of variation within the tachocline as compared to the models we are using for the fits, we do not expect the thickness of tachocline as determined by our procedure to agree with the actual thickness.

Comparing the region in which the rotation rate varies from $1/(1+e)$ to $1 - 1/(1+e)$ of the total jump, it appears that the effective width in the test model is about 3.25 times less than what is given by equation (20), when models with form given by equation (17) are used. Thus the estimated values should be compared with this scaled width as has been done in Fig. 8. Apart from the form of variation within the tachocline, the trend in the lower CZ in test model is also far from linear and hence may not be properly modelled by the tachocline model used in annealing fits. Note that all the results are roughly within the error bars of the exact values, even though the form of variation within the tachocline as well as the trend in the CZ in the test model are different from those in the calibration models. If we use a test model with the same form for tachocline as used in the calibration models it is possible to obtain much better results. This gives us confidence that we can indeed determine the parameters of the solar tachocline.

The variation in the position and thickness of tachocline with latitude is not totally clear from the estimated parameters, since these variations were chosen to be comparable to the error estimates as happens to be the case for observed splittings also. It appears that a variation of $0.02R_\odot$ in position of tachocline is barely at the limits of detection with the present data. The variation in thickness is not very evident as the estimated thickness appears to be too small at all latitudes.

Having tested our techniques on a test model we now apply the same procedure to the GONG data for the months 4–10 and 4–14. Fig. 9 shows the process of determining the tachocline parameters for the solar equator. The results obtained using the calibration methods are listed in Table 1. A positive jump implies a rotation rate which is higher in the CZ than in the radiative interior. From Table 1 we note that the results for the two data sets are consistent with each other within the estimated errors. However, the GONG months 4–10 data have larger error as compared to the months 4–14 data and that is reflected in the larger errors in the tachocline parameters. We thus focus our attention on results for data from GONG months 4–14, which have also been used in the method of simulated annealing.

The change in the tachocline jump as a function of latitude is very clear. This is not surprising since the change is large enough to be seen by normal inversions also. The result obtained seems to depend somewhat on the type of calibration model used, although at each latitude they are consistent within errors. It also appears that the results are more sensitive to data errors when models with a flat rotation-rate in the CZ are used. This is perhaps not surprising as the jump at each latitude is not assumed to be known beforehand, while for the models with trend, a first estimate of the jump is made from the inversion results and only a correction-factor is obtained by the fit in equation (13). The estimated errors in position and thickness at all latitudes are larger than the corresponding errors in mean values as estimated by Basu (1997) using only the splitting coefficient c_3. This is partly due to the fact that the error estimates in splittings for each latitude is larger than those in c_3 alone. Further, a large part of the variation in tachocline is determined by c_3, which shows a clear jump around the tachocline, and at the same time has very little variation in the CZ or in radiative interior thus making it much easier
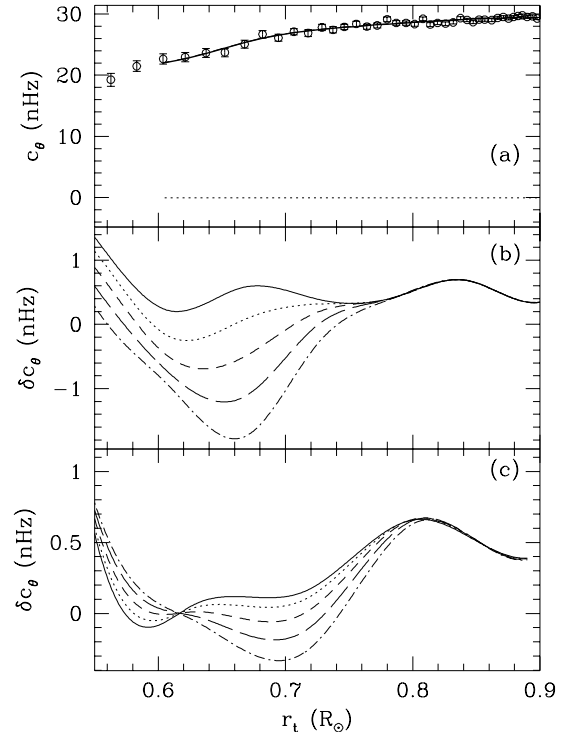

Figure 9. (a) Calibration for determining the jump in the rotation rate in tachocline. The points are the splitting-coefficients combination for the equator with the contribution from Ω_c removed. The continuous line is the fit to the data, which can be decomposed into two parts — the dotted line which is the term $\phi(r_t)$ in equation (13) and the dashed line which is the calibration model scaled to the fitted jump (term $\alpha a_\theta(r_t)$). The data used are the GONG4–14 splittings. The dashed and continuous lines more or less coincide in this case. (b) The spline representation of the difference between the data shown above and the the five calibration models used to determine the tachocline position. The continuous, dotted, small-dashed, long-dashed and dot-dashed lines are difference with calibration models for $r_d = 0.68$, 0.69, 0.70, 0.71 and $0.72R_\odot$ respectively. All these calibration models have $w = 0.005R_\odot$ (c) The spline representation of the difference between the data and the five calibration models used to determine the tachocline width. The continuous, dotted, small-dashed, long-dashed and dot-dashed lines are difference with calibration models for $w = 0.005$, 0.01, 0.015, 0.02 and $0.025R_\odot$ respectively. These calibration models have $r_d = 0.69R_\odot$.

to fit the tachocline parameters.

There appears to be a slight variation in the radial position of the tachocline with the tachocline moving outwards at higher latitudes. However, the change is not very significant – being only about 1σ between the equator and $60°$ latitude. But the results seem to indicate a nearly systematic shift.

The question about variation in the thickness is less clear, however. In fact for all latitudes, it appears that the thickness is very small and comparable to the error estimates. Thus better data with reduced errors are required before the thickness can be determined reliably. With this method, at the moment we can only put an upper limit on the thickness of the tachocline at all latitudes. Basu (1997) had shown that the thickness measurements are somewhat sensitive to the calibration models used. Thus we should try to check these results against those obtained by the tech-

Table 1. Solar tachocline parameters as determined by calibration

Lat. (°)	Calibration models with flat CZ			Calibration models with trend in CZ		
	Jump (nHz)	Position ($R_\odot$)	Half-width ($R_\odot$)	Jump (nHz)	Position ($R_\odot$)	Half-width ($R_\odot$)
	GONG months 4–10 data					
0	21.66 ± 2.57	0.6921 ± 0.0142	0.0134 ± 0.0120	20.92 ± 2.46	0.6954 ± 0.0113	0.0029 ± 0.0120
15	18.52 ± 1.91	0.6941 ± 0.0111	0.0124 ± 0.0137	18.11 ± 0.92	0.6891 ± 0.0115	0.0190 ± 0.0131
45	-27.81 ± 2.30	0.6863 ± 0.0277	0.0215 ± 0.0173	-27.17 ± 2.06	0.6903 ± 0.0263	0.0170 ± 0.0172
60	-60.47 ± 3.52	0.7025 ± 0.0117	0.0070 ± 0.0075	-60.08 ± 1.33	0.6990 ± 0.0099	0.0050 ± 0.0077
75	-86.41 ± 9.99	0.6968 ± 0.0224	0.0094 ± 0.0129	-89.04 ± 2.56	0.6974 ± 0.0238	0.0123 ± 0.0135
	GONG months 4–14 data					
0	19.39 ± 2.00	0.6944 ± 0.0096	0.0079 ± 0.0130	21.52 ± 0.82	0.6851 ± 0.0077	0.0047 ± 0.0083
15	18.13 ± 1.55	0.6996 ± 0.0091	0.0083 ± 0.0106	18.29 ± 0.89	0.6922 ± 0.0097	0.0043 ± 0.0087
45	-28.89 ± 2.66	0.7077 ± 0.0137	0.0047 ± 0.0061	-29.87 ± 2.22	0.7048 ± 0.0148	0.0059 ± 0.0067
60	-57.18 ± 4.11	0.7058 ± 0.0098	0.0031 ± 0.0055	-57.10 ± 1.51	0.7082 ± 0.0072	0.0051 ± 0.0062
75	-88.21 ± 6.70	0.7204 ± 0.0183	0.0154 ± 0.0235	-87.15 ± 1.78	0.7162 ± 0.0178	0.0141 ± 0.0136

Table 2. Tachocline parameters from 1D-annealing

Lat. (°)	Jump (nHz)	Position ($R_\odot$)	Half-width ($R_\odot$)	χ^2
0	17.20 ± 4.96	0.6843 ± 0.0112	0.0020 ± 0.0019	1.0401
15	14.84 ± 1.52	0.7146 ± 0.0050	0.0028 ± 0.0022	1.1271
30	-7.46 ± 1.71	0.7193 ± 0.0196	0.0242 ± 0.0136	0.9860
45	-33.83 ± 3.90	0.7160 ± 0.0072	0.0122 ± 0.0073	0.9276
60	-59.86 ± 6.19	0.7045 ± 0.0061	0.0089 ± 0.0078	1.0712
75	-91.19 ± 3.36	0.6878 ± 0.0089	0.0216 ± 0.0095	1.1762

nique of simulated annealing.

In order to obtain an independent measure of variation in properties of tachocline with latitude, we adopt the technique of simulated annealing to fit the tachocline parameters to the GONG months 4–14 data for different latitudes. Fig. 10 shows the 1D annealing result for the equator. Note that we get a good fit and the residuals are random and consistent with the error estimates. The 1D annealing results for various latitudes are listed in Table 2. As in the case of the calibration technique, the jump shows a clear change with latitude, although there appears to be some systematic difference between the value of the jump obtained by the two techniques. All the values appear to be reduced in annealing results as compared to the corresponding values obtained by the calibration method, although for individual latitudes the results are generally within error limits from those obtained using calibration method. The reason for this discrepancy is not altogether obvious, but there may be some ambiguity in the definition of jump as a part of the variation across the tachocline may be accounted for by the smooth trend, defined by the term involving B in equation (17). Note from the last column which gives the χ^2 per degree of freedom, it is clear that the fit is reasonably good as all the values are close to unity.

The results at $30°$ latitude are not particularly reliable as the jump is too small to define the tachocline properly and hence the errors are very large. At high latitudes although the splittings have larger error, the increase in magnitude of jump makes the tachocline better defined and in some cases the error estimate also reduces since the fits are more stable. At low latitudes, however, there is some problem in finding a proper fit, as the estimated values have a larger
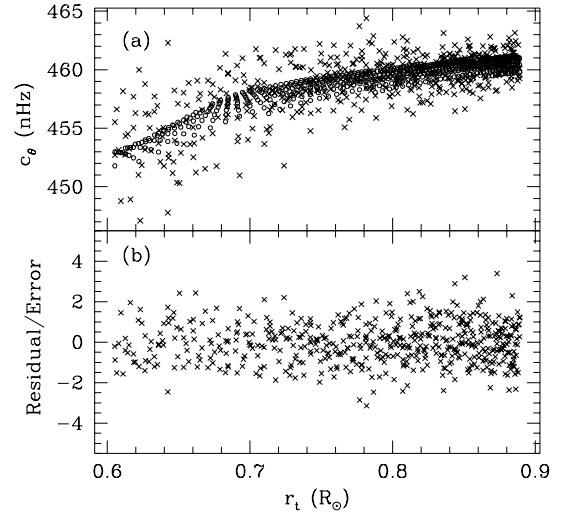
Figure 10. The 1D simulated annealing results for the solar equator. In Panel (a) The crosses are the observed splitting combinations and the circles are those obtained by the fit. Panel (b) shows the normalised residuals.

scatter, which is reflected in comparatively large errors even though the errors in splitting coefficients is lowest for these latitudes. This could be due to the fact that the form of trend assumed in the tachocline model defined by equation (17) is not sufficient to model the variation in rotation rate. As can be seen from the contour diagram in Fig. 3, there is some variation at low latitudes in the convection zone, which perhaps cannot be modelled properly by a linear trend.

The annealing results also indicate that the thickness of the tachocline is very small at low latitudes. The thickness appears to increase at higher latitudes though the estimated errors also increase and it is not clear if the increase is significant. Similarly, it is not clear if shift in the tachocline position with latitude is also significant, though in general once again the tachocline appears to shift to slightly larger radial distance at higher latitudes.

We feel that there should be yet another independent test of the significance of variation in tachocline position and thickness with latitude. We have therefore tried a 2D annealing fit to simultaneously determine all the parameters at all
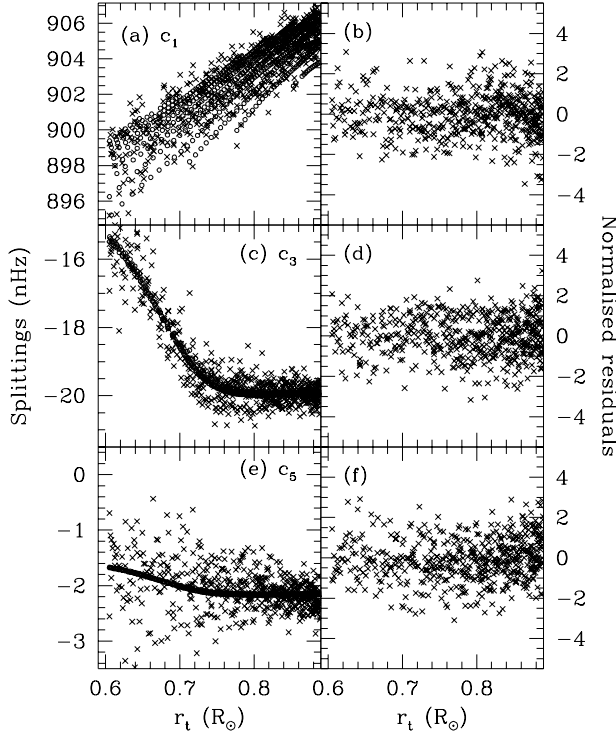
Figure 11. The fit to the first three splittings coefficients and the normalized residuals of the fits obtained by the 2D simulated annealing method assuming that there is no latitudinal variation in the position and thickness of the tachocline.

Figure 12. Same as Fig. 11, but with the possible latitudinal variation in the position and thickness of the tachocline taken into account

latitudes. Since this fit involves 12 parameters as defined by equations (17),(18), it is not clear if all of them are required. For verifying this we start with the simplest situation where the position and width of tachocline are independent of latitude (i.e., $r_{d3} = 0$, $w_3 = 0$). This fit yields the mean position of tachocline as $0.7038R_\odot$ and a half-width of $0.0187R_\odot$ and the fit is shown in Fig. 11. These values are consistent with the results obtained by Basu (1997), though the half-width is slightly higher than the value found by Basu (1997). Some of the difference may arise because while Basu (1997) used only the splitting coefficient c_3 to determine the tachocline parameters, in this work we are using the first three splitting coefficients. If this difference is significant it may imply a latitudinal variation in tachocline position or width. Further, this fit has a $\chi^2 = 1.108$ per degree of freedom and the fit appears to be reasonably good. When all 12 parameters are included in the fit the minimum χ^2 per degree of freedom reduces to 1.088. Thus the reduction in χ^2 is only marginal and it is tempting to conclude that the GONG months 4–14 data are consistent with no latitudinal variation in position or width of the tachocline. Of course, we can not rule out a small variation in the tachocline properties with latitude. Monte-Carlo simulation with 12 parameters yields the following results for the tachocline:

$$r_d = [(0.6991 \pm 0.0099) + (0.0030 \pm 0.0061)P_3(\theta)]R_\odot,$$
$$w = [(0.0084 \pm 0.0072) + (0.0047 \pm 0.0042)P_3(\theta)]R_\odot,$$
$$\delta\Omega = (-1.83 \pm 2.18) - (22.71 \pm 1.01)P_3(\theta)$$
$$- (3.88 \pm 0.45)P_5(\theta) \text{ nHz}, \tag{21}$$

It is clear that the variation in position is at a level of $(1/2)\sigma$ only, while the thickness at all latitudes is comparable to the
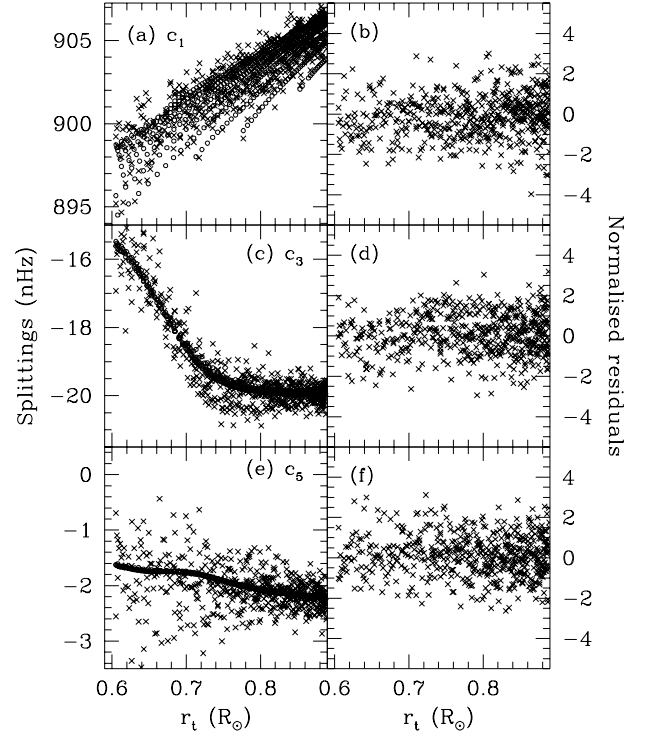
error estimates and as such it is not clear if the variation in thickness is significant. Similarly, the first component of $\delta\Omega$ is also not significant. In fact, we find that if this parameter is set to zero, the fit is more stable in the sense that the χ^2 reduces to acceptable level in most of the attempts with simulated annealing and as such we prefer to use that fit. The minimum value of χ^2 per degree of freedom in this case is 1.105 and the resulting parameters of the tachocline are

$$r_d = (0.6947 + 0.0035P_3(\theta))R_\odot,$$
$$w = (0.0067 + 0.0014P_3(\theta))R_\odot, \tag{22}$$
$$\delta\Omega = -21.11P_3(\theta) - 2.96P_5(\theta) \text{ nHz},$$

while the fit is shown in Fig. 12. We adopt these values for the tachocline model for use in the next section and for comparison with other estimates. It is clear that addition of two parameters determining the variation in properties with latitude does not improve the fit significantly and hence there is no compelling reason to believe that there is any variation in position or thickness of tachocline with latitude. Nevertheless, all the results which attempt to determine the variation find an increase in thickness with latitude and a shift outwards in the mean position of tachocline with increasing latitude. Although this variation does not appear to be significant in terms of the expected errors, a small variation in properties of the tachocline with latitude cannot be ruled out.

Fig. 13 summarizes the results from all the techniques. This figure shows the variation in jump, position and thickness of the tachocline as obtained by different techniques from the GONG months 4–14 data. We have chosen the results from calibration method using the models with trend for this purpose. It is clear that there is a general agreement
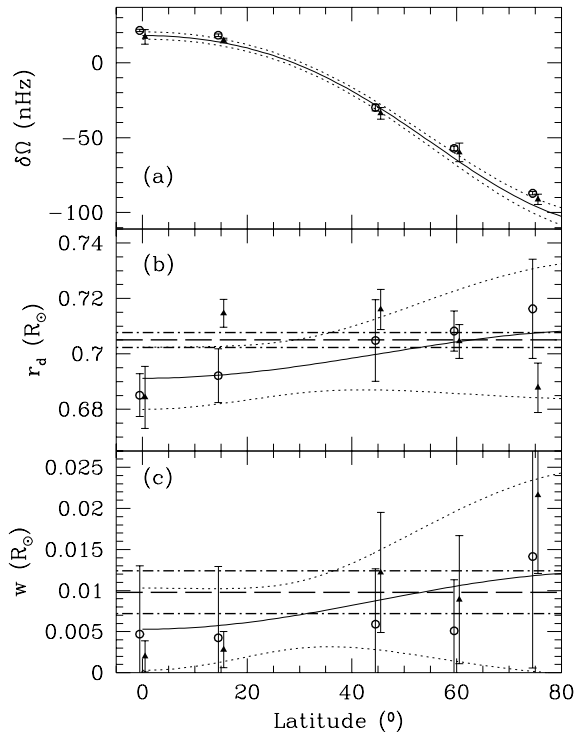
Figure 13. A summary of the tachocline results obtained using the GONG months 4–14 data. Panels (a),(b) and (c) show the results of the jump, position and thickness respectively. In each panel the continuous line is the results of the 2D annealing (equation 18) with the 1σ error bounds shown as the dotted lines. The circles show the results of the calibration method and the triangles are the results obtained by 1D annealing. The symbols are displaced by $\pm 0.5°$ about the true latitude for the sake of clarity. The dashed line in panels (b) and (c) mark the mean values found by Basu (1997), while the 1σ error bounds are shown as dot-dashed lines.

between the three independent results at most latitudes and all these results point to an increase in thickness with latitude as well as an outward radial shift in the position of tachocline with latitude. This figure also shows the mean position and width of tachocline as determined by Basu (1997) and it appears that all the results are also consistent with no latitudinal variation in position or width of tachocline. Clearly, better data is required to find any possible variation in tachocline properties with latitude.

4 INVERSION AFTER REMOVING THE TACHOCLINE SIGNAL

The smoothing used in our inversion procedure tends to smooth out the steep variation in rotation rate in the tachocline. Apart from this it may also introduce some ripples away from the position of tachocline, a feature that is reminiscent of the Gibbs phenomenon in Fourier transform. In order to overcome this limitation and to use the tachocline parameters determined in the earlier section for improving the results of inversion, we attempt an inversion after removing the signal from tachocline. For this purpose we adopt tachocline parameters given by equation (22), leaving aside the smooth part and perform a forward calculation to obtain the splitting coefficients for this model. These splittings
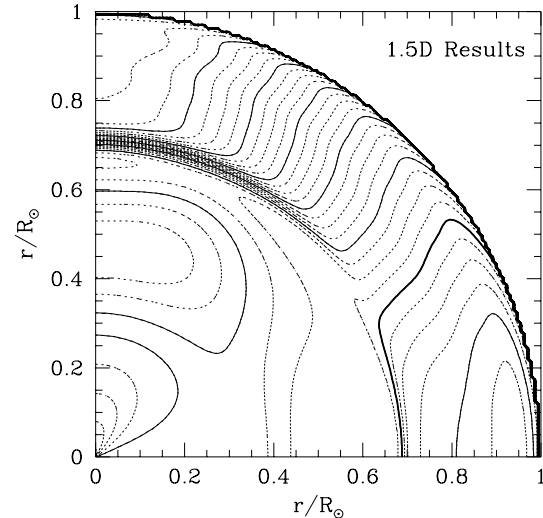
Figure 14. A contour diagram of the solar rotation rate as obtained by 1.5D inversion of the GONG months 4–14 data after removal of the tachocline. The format is the same as that for Fig. 3.

are then subtracted from the observed splittings before inverting the data. The rotation rate in the tachocline model is then added to the inverted profile to obtain the actual rotation rate in the Sun.

The results in Fig. 14 display the contour diagram for the rotation rate obtained using 1.5D inversion, while Fig. 15 shows the rotation rate as a function of radial distance at selected latitudes for the inversions with and without removal of tachocline. From this figure it appears that at the $30°$ latitude the results obtained using the 2D inversion after removing the tachocline are different from other results. The reason for this difference are not altogether clear, though it appears to manifest at latitudes around the region where the radial gradient in the tachocline changes sign. The results obtained after removing the tachocline appear to be smoother in general, which is of course, not surprising. Also, the fact that the simulated annealing was able to obtain a good fit over a large fraction of radial distance using only 12 parameters suggests that there is probably not much structure in the rotation rate as a function of latitude or radial distance (apart from tachocline itself) in the region $0.6 < r/R_\odot < 0.9$. However, from the 2D annealing fits there are reasons to believe that these 12 parameters are not completely adequate to represent the trends at all latitudes adequately. Nevertheless, it is likely that some features seen in the lower part of CZ in certain inversion results (e.g., Figs. 3,4) are due to the influence of tachocline magnified by errors in data.

5 CONCLUSIONS

In this work we have attempted to infer the rotation rate inside the Sun using observed p-mode frequency splittings. We have used a 1.5D inversion technique to invert the data in the form of splitting coefficients based on a regularized least squares method with iterative refinement. We have investigated the influence of using different prescription for smoothing to find that the differences are comparable to expected errors in inversion results. Similarly, an adoption of
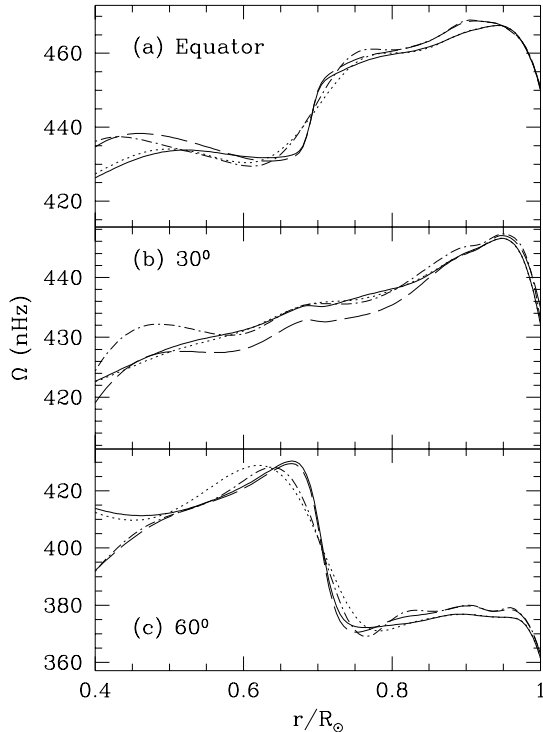
Figure 15. A comparison of the inversion results with and without removal of tachocline. Continuous line shows the results obtained using 1.5D inversion after removing the tachocline contribution, the dotted line is the 1.5D result of normal inversion. Similarly, the dashed line show the results of 2D inversion of individual splittings after removing the tachocline while the dot-dashed line shows the results from normal 2D inversion.

different sets of observed splitting coefficients shows that the difference in various results is again roughly consistent with error estimates based on quoted errors in observed splittings. Apart from the 1.5D inversion technique, we have also attempted 2D inversion for both the individual splittings $D_{n,\ell,m}$ and the splitting coefficients $c_s^{(n,\ell)}$. All these results agree reasonably well inside the convection zone, although in the deep interior there are some differences between different inversion results. We believe these reflect our inability to obtain reliable estimate of rotation rate in the core due to possible systematic errors in splittings for low degree modes.

It is clear from our results that the surface differential rotation persists through the solar convection zone, while below the base of convection zone the rotation rate appears to be relatively independent of latitude. The transition around the base of the convection zone may not be resolved by the inversion results. The core appears to be rotating slower than the surface equatorial rotation rate as also found by Tomczyk, Schou & Thompson (1995) and Elsworth et al. (1995). The rotation rate in solar core has been recently discussed by Gizon et al. (1997) and Rabello-Soares et al. (1997) and it appears that there is significant variation in the inferred rotation rate in the solar core from different helioseismic data. The constraints on the rotation rate in the core in the form of the boundary conditions (8), in the 1.5D inversion make the core rotate essentially as a rigid body and reduces the discrepancy in rotation rate inferred using different data sets. This may be artificial, but unfortunately we do not have enough data to resolve any variation

in rotation rate in the core and this is probably the simplest assumption that we can make (Chaplin et al. 1996). Even a small error in splittings for low degree modes can change the inverted rotation rate in the core significantly if no constraints are applied. Further, as can be seen from Fig. 1, the results outside the core are not too sensitive to the point where these boundary conditions are applied or the form of smoothing used. The main problem with reliable inversion of rotation rate in the core is that the low degree modes that penetrate into the core have large errors in the splitting coefficients (possibly including some systematic errors), and this allows for a wide range of rotation profiles in the core. It is clear that better quality data are required to make any reliable estimate of rotation rate in the solar core.

Further, there is a distinct shear layer just underneath the solar surface where the rotation rate increases with depth. There is also a hint of this shear layer becoming less pronounced with latitude, in the sense that the radial variation of the rotation rate tends to diminish with increasing latitude. The rotation rate has a maximum around $r = 0.95R_\odot$ at most latitudes, except possibly close to the poles. This feature can also be seen in the raw splitting data (Fig. 7). The inferred rotation rate at the solar surface agrees reasonably well with that obtained from Doppler measurements (Snodgrass 1992). Some differences between the Doppler measurement and inverted profile (Fig. 6) at higher latitudes could be because the Doppler measurements determine only terms up to $\cos^4 \theta$ in expansion of rotation rate. The higher order terms included in inversions will contribute significantly at high latitudes.

The tachocline or the shear layer near the base of convection zone has been studied in detail using forward techniques to ascertain possible latitudinal variation in its properties. Since the tachocline cannot be resolved by inversions, we have used a number of forward modelling techniques to study the tachocline. With the present data, we do not find any compelling evidence for any variation in the position or thickness of the tachocline with latitude. The mean position and thickness of tachocline is found to be consistent with the values found by Basu (1997). Our results suggest that the thickness increases marginally with latitude and the location of tachocline also appears to shift outwards with increasing latitude, but the difference between the position and thickness of the tachocline at the solar equator and at a latitude of $60°$ is comparable to the estimated errors. It is therefore, not clear if the variation is really significant. Similarly, the 2D annealing results also show that the variations in the position and thickness are less than the respective error bars. Further, there is no significant reduction in the χ^2 for the fit when the variation of position and width with latitude is included in the 2D fits. Taking the errors into account we believe that we get an upper limit of $0.03R_\odot$ for the variation in the position of the tachocline and about $0.02R_\odot$ for the variation of the thickness. Clearly, more precise data are needed to make a better estimate of the parameters reliably.

From our results it appears that the tachocline is centered at a depth which is below the base of the solar convection zone at all latitudes. If the latitudinal variation shown by our results is real then at low latitudes most of the variation in rotation rate within the tachocline occurs below the CZ base, while at high latitudes part of the tachocline may extend into the convection zone.

ACKNOWLEDGMENTS

REFERENCES

Antia H. M., Chitre S. M., 1996, Bull. Astron. Soc. India, 24, 375

Antia H. M., Chitre S. M., Thompson M. J., 1996, A&A, 308, 656

Basu S., 1997, MNRAS, 288, 572

Brown T. M. Christensen-Dalsgaard J., Dziembowski W. A., Goode P. R., Gough D. O., Morrow C. A., 1989, ApJ, 343, 526

Chaplin W. J., Elsworth Y., Howe R., Isaak G. R., McLeod C. P., Miller B. A., New R., 1996, MNRAS, 280, 849

Charbonneau P., Christensen-Dalsgaard J., Henning R., Schou J., Thompson M. J., Tomczyk S., 1997, in eds., Provost J., Schmider F. -X., IAU Symp. 181: Sounding Solar and Stellar Interiors, Posters Volume, Kluwer, Dordrecht, (in press)

Corbard T., Berthomieu G., Morel P., Provost J., Schou J., Tomczyk S., 1997, A&A, 324, 298

Elsworth Y., Howe R., Isaak G. R., McLeod C. P., Miller B. A., New R., Wheeler S. J., Gough D. O., 1995, Nature, 376, 669

Gilman P. A., Fox P. A., 1997, ApJ, 484, 439

Gizon L., Fossat E., Lazrek M. et al., 1997, A&A, 317, L71

Gough D. O., Thompson M. J. 1991, in *Solar Interior and Atmosphere,* eds., Cox A. N., Livingston W. C., Matthews M., Space Science Series, University of Arizona Press, p519

Hill F., Stark P. B., Stebbins R. T. et al., 1996, Science, 272, 1292

Kosovichev A. G., 1996, ApJ, 469, L61

Kosovichev A. G., Schou J., Scherrer P. H. et al., 1997, Solar Phys., 170, 43

Pijpers F. P., 1997, A&A, (in press)

Pijpers F. P., Thompson M. J., 1992, A&A, 262, L33

Press W. H., Flannery B. P., Teukolsky S. A., Vetterling W. T., 1993, in Numerical Recipes, 2nd Edition (Cambridge: Cambridge Univ. Press).

Rabello-Soares M. C., Rocacortes T., Jimenez A., Appourchaux T., Eff-Darwich A., 1997, ApJ 480, 840

Richard O., Vauclair S., Charbonnel C., Dziembowski W. A., 1996, A&A, 312, 1000

Ritzwoller M. H., Lavely E. M., 1991, ApJ, 369, 557

Rüdiger G., Kitchatinov L. L., 1996, ApJ, 466, 1078

Schou J., Christensen-Dalsgaard J., Thompson M. J., 1994, ApJ, 433, 389

Sekii T., 1993, MNRAS, 264, 1018

Snodgrass H. B., 1992, in The Solar Cycle, ed. Harvey K. L., Astron. Soc. Pacif. conf. Ser. Vol. 27, p 205

Spiegel E. A., Zahn J.-P., 1992, A&A, 265, 106

Thompson M. J., Toomre J., Anderson E. R., et al., 1996, Science, 272, 1300

Tomczyk S., Schou J., Thompson M. J., 1995, ApJ, 448, L57

Vanderbilt D., Louie S. G., 1984, J. Comp. Phys., 56, 259

Weiss N. O., 1994, in eds. Proctor M. R. E, Gilbert A. D., Lectures on Solar and Planetary Dynamo, Cambridge Univ. Press, p59

Wilson P. R., Burtonclay D., 1995, ApJ, 438, 445

Wilson P. R., Burtonclay D., Li Y., 1996, ApJ, 470, 621

Woodard M. F., Libbrecht K. G., 1993, ApJ, 402, L77